Neutral Higgs-Boson Pair Production at Hadron Colliders: QCD Corrections

S. Dawson[1], S. Dittmaier[2] and M. Spira[*][3]

[1] *Physics Department[†], Brookhaven National Laboratory, Upton, NY 11973, USA*

[2] *Theory Division, CERN, CH–1211 Geneva 23, Switzerland*

[3] *II. Institut für Theoretische Physik[‡], Universität Hamburg, Luruper Chaussee 149, D–22761 Hamburg, Germany*

Abstract

Neutral Higgs-boson pair production provides the possibility of studying the trilinear Higgs couplings at future high-energy colliders. We present the QCD corrections to the gluon-initiated processes in the limit of a heavy top quark in the loops and the Drell–Yan-like pair production of scalar and pseudoscalar Higgs particles. The *pp* cross sections are discussed for LHC energies within the Standard Model and its minimal supersymmetric extension. The QCD corrections are large, enhancing the total cross sections significantly.

---

1 Introduction

The Higgs mechanism is a cornerstone of the Standard Model (SM) and its supersymmetric extensions. Thus, the search for Higgs bosons is one of the most important endeavours at future high-energy experiments. In the SM one Higgs doublet, Φ, has to be introduced in order to break the electroweak symmetry, leading to the existence of one elementary Higgs boson, H [1]. The scalar sector of the SM is uniquely fixed by the vacuum expectation value v of the Higgs doublet and the mass M_H of the physical Higgs boson [2]. Once a Higgs particle is found, it is necessary to investigate its properties in order to reconstruct the Higgs potential and to verify that it is indeed the SM Higgs boson. A first step in this direction is the measurement of the trilinear self-couplings, which are uniquely specified by the scalar potential

$$V = \lambda \left(\Phi^\dagger \Phi - \frac{v^2}{2} \right)^2. \tag{1}$$

The parameter λ defines the strength of the Higgs self-interactions. In the SM it is given by $\lambda = M_H^2/(2v^2)$. At tree level, λ can only be probed through multiple Higgs-boson interactions and there are, at present, no direct experimental limits on λ. In extensions of the SM, such as models with an extended scalar sector, with composite particles or with supersymmetric partners, the self-couplings of the Higgs boson may be significantly different from the SM predictions. The limits that may be obtained on the trilinear self-coupling of the Higgs boson at the LHC and the impact of QCD corrections represent a particular topic of this paper.

Since the minimal supersymmetric extension of the Standard Model (MSSM) requires the introduction of two Higgs doublets in order to preserve supersymmetry, there are five elementary Higgs particles, two $\mathcal{CP}$-even (h, H)[1], one $\mathcal{CP}$-odd (A) and two charged ones $(H^\pm)$. This leads to a large variety of self-interactions among them. At lowest order all couplings and masses of the MSSM Higgs sector are fixed by two independent input parameters, which are generally chosen as $\mathrm{tg}\beta = v_2/v_1$, the ratio of the two vacuum expectation values $v_{1,2}$, and the pseudoscalar Higgs-boson mass M_A. The self-interactions among the Higgs bosons (at lowest order) are given in terms of the electroweak gauge couplings, $\mathrm{tg}\beta$ and M_A, and may be quite different from the ones of the SM, which are governed by the parameter λ. Higher-order corrections to the MSSM Higgs sector turn out to be important owing to the large top-quark mass m_t [3–5]. They increase the upper bound on the light scalar Higgs mass M_h from the Z-boson mass M_Z to about 130 GeV, along with altering the Higgs-boson self-couplings with contributions proportional to $G_F m_t^4/M_Z^2$.

Higgs-boson pairs can be produced by several mechanisms at hadron colliders:

- Higgs-strahlung $W^*/Z^* \to \phi_1 \phi_2 W/Z$ [6],

- vector-boson fusion $WW, ZZ \to \phi_1 \phi_2$ [7],

- associated production $Z^* \to Ah, AH,$

---

[1]We have taken care that no confusion can arise from using the same symbol H for the SM and the heavy $\mathcal{CP}$-even MSSM Higgs particle.

- Higgs radiation off top and bottom quarks $gg, q\bar{q} \to Q\bar{Q}\phi_1\phi_2$ [8],

- gluon–gluon collisions $gg \to \phi_1\phi_2$ [9, 10].

At the LHC, gluon fusion is the dominant source of Higgs-boson pairs, although in some regions of the MSSM parameter space, vector-boson fusion [11] can be important. Note, however, that $gg \to HA$ represents an exceptional case, since this channel is suppressed with respect to the Drell–Yan-like process $q\bar{q} \to Z^* \to HA$, so that it will be very difficult to separate the gluon-fusion process in this case experimentally. The gluon-fusion process $gg \to hA$, on the other hand, is competitive with the Drell–Yan-like process $q\bar{q} \to Z^* \to hA$.

In this paper we present the QCD corrections to the Drell–Yan-like production and the gluon–gluon collision processes. The gluon-fusion processes are, in the SM, mediated by triangle and box loops of top and bottom quarks; in the SM, the contributions of the bottom quark can always be neglected. In the MSSM, the squark contributions will be suppressed if the squarks are heavier than ~ 400 GeV, and, for small tgβ, the top-quark loops dominate the gg cross sections. The QCD corrections to the gluon-fusion processes have been obtained in the limit of a heavy top quark by means of low-energy theorems and also by explicitly expanding all relevant one- and two-loop diagrams. The results are expected to be valid for small tgβ in the MSSM and below the $t\bar{t}$ threshold of the top-quark loops in both the MSSM and the SM, since in this regime effects of a finite top-quark mass are expected to be small. In the case of single-Higgs production the same procedure reproduces the known exact result for the NLO cross section within 5%, for Higgs-boson masses below $2m_t$ [12]. The considered QCD corrections are important in the process of extracting limits on the Higgs-boson self-couplings reliably.

The paper is organized as follows. In the next section the low-energy theorems for the interactions of gluons with light Higgs bosons will be reviewed, and the relevant interactions in the heavy-quark limit will be constructed. In Section 3 the details of the calculation will be described, and in Section 4 we present the results for the SM and MSSM Higgs bosons. In Section 5 we give some conclusions.

2 Low-Energy Theorems

In the low-energy limit of vanishing Higgs four-momentum, the Higgs-field operator acts as a constant field. In this limit it is possible to derive an effective Lagrangian for the interactions of the Higgs bosons with gauge bosons, which is valid for light Higgs bosons. This effective Lagrangian has been successfully used to compute the QCD corrections to a number of processes, in particular to single-Higgs production from gluon fusion at the LHC [13, 14]. In this case, the result of using the low-energy theorems has been shown to agree with the exact two-loop calculation to better than 10% even for M_H as large as 1 TeV. This lends legitimacy to our use of the low-energy theorems to compute QCD corrections to multiple Higgs-boson production via gluon fusion.

3

In the limit of vanishing Higgs four-momentum the entire interaction of the scalar Higgs particles H_i with a heavy quark Q can be generated by the substitution

$$m_Q^0 \to m_Q^0 + \eta_Q^0 \sum_i g_Q^i H_i \tag{2}$$

in the Lagrangian of a heavy quark of bare mass m_Q^0 [15], where $\eta_Q^0 = m_Q^0/v$ denotes the bare SM Yukawa coupling, which must not be included in the substitution. The symbol g_Q^i is the relative strength of the heavy-quark Yukawa coupling,

$$\mathcal{L}_{\text{Yuk}} = -\eta_Q \sum_i g_Q^i \overline{Q} Q H_i. \tag{3}$$

In the SM, we have $g_Q^i = 1$. The expressions for g_Q^i in the MSSM are given in Ref. [14]. At higher orders this substitution has to be performed for the unrenormalized parameters [14, 16]. In the following we restrict our analysis to the top-quark contributions. At next-to-leading order (NLO) the effective interaction between several scalar Higgs fields and gluons can be obtained from the radiatively corrected effective Lagrangian of gluon fields,

$$\mathcal{L}_{gg} = -\frac{1}{4} G^{a\mu\nu} G_{\mu\nu}^a \left[1 + \Pi_{gg}^t(0) \right], \tag{4}$$

with $\Pi_{gg}^t(0)$ denoting the top-quark contribution to the unrenormalized gluon vacuum polarization at zero-momentum transfer. At two-loop order, we have

$$\Pi_{gg}^t(0) = \frac{\alpha_s^{(5)}}{\pi} \Gamma(1+\epsilon) \left(\frac{4\pi\mu^2}{(m_t^0)^2} \right)^\epsilon \left\{ \frac{1}{6\epsilon} + \frac{\alpha_s^{(5)}}{\pi} \Gamma(1+\epsilon) \left(\frac{4\pi\mu^2}{(m_t^0)^2} \right)^\epsilon \left[\frac{1}{16\epsilon} + \mathcal{O}(\epsilon^0) \right] + \mathcal{O}(\alpha_s^2) \right\}, \tag{5}$$

where the strong coupling constant $\alpha_s^{(5)}$ includes five light flavours. This means that the top-quark contribution to the running of α_s has been subtracted at vanishing momentum transfer. Hereafter, we drop the superscript 5 on α_s. Performing the substitution Eq. (2) and renormalizing the bare top mass m_t^0 via

$$m_t^0 = m_t \left[1 - \frac{\alpha_s}{\pi} \Gamma(1+\epsilon) \left(\frac{4\pi\mu^2}{m_t^2} \right)^\epsilon \left(\frac{1}{\epsilon} + \frac{4}{3} \right) + \mathcal{O}(\alpha_s^2) \right], \tag{6}$$

where m_t denotes the pole mass, we end up with the NLO result

$$\mathcal{L}_{H^n gg} = \frac{\alpha_s}{12\pi} G^{a\mu\nu} G_{\mu\nu}^a \log \left[1 + \sum_i g_t^i \frac{H_i}{v} \right] \left\{ 1 + \frac{11}{4} \frac{\alpha_s}{\pi} \right\}. \tag{7}$$

The interaction of even numbers of pseudoscalar Higgs bosons with gluons can be determined analogously from Eq. (5) by substituting [16]

$$(m_t^0)^2 \to (m_t^0)^2 + (g_t^A \eta_t^0 A)^2, \tag{8}$$

leading to

$$\mathcal{L}_{A^{2n} gg} = \frac{\alpha_s}{24\pi} G^{a\mu\nu} G_{\mu\nu}^a \log \left[1 + \left(g_t^A \frac{A}{v} \right)^2 \right] \left\{ 1 + \frac{11}{4} \frac{\alpha_s}{\pi} \right\}. \tag{9}$$

4

The case of odd numbers of pseudoscalar Higgs bosons can be derived from the ABJ anomaly [17] in the divergence of the axial vector current [14, 16, 18]. The interactions that are relevant in our case are[2]

$$\mathcal{L}_{Agg} = g_t^A \frac{\alpha_s}{8\pi} G^{a\mu\nu} \tilde{G}_{\mu\nu}^a \frac{A}{v},$$

$$\mathcal{L}_{AHgg} = -g_t^A g_t^H \frac{\alpha_s}{8\pi} G^{a\mu\nu} \tilde{G}_{\mu\nu}^a \frac{AH}{v^2}, \tag{10}$$

where $\tilde{G}_{\mu\nu}^a = \frac{1}{2}\epsilon_{\mu\nu\alpha\beta}G^{a\alpha\beta}$ denotes the dual gluon field-strength tensor. Owing to the Adler–Bardeen theorem [19] there are no higher-order corrections to the effective Lagrangians involving odd numbers of pseudoscalar Higgs bosons.

Figure 1 summarizes the Feynman rules for the effective interactions between two gluons and one or two Higgs bosons; the rules can be read off from Eqs. (7)–(10). These Feynman rules can now be used to compute Higgs interactions beyond the lowest order. We recall that there is no contribution of light quarks (which are considered to be massless) to the effective couplings, but note that light-quark loops have to be included when the Higgs bosons do not directly couple to the quark loops. Such contributions arise, in particular, in $gg \to Z^* \to hA, HA$ and cannot be obtained from the low-energy theorems.

3 QCD Corrections

3.1 Gluon fusion: basic definitions

At leading order (LO) neutral-Higgs pair production via gluon fusion is mediated by triangle and box diagrams of heavy quarks, as exemplified in Fig. 2. In the heavy-quark limit, the fermion triangles and boxes can be replaced by the effective vertices of Fig. 1. Throughout this analysis, we choose the squark masses to be 1 TeV so that squark-loop contributions can be neglected in the MSSM case. Generically the partonic LO cross section can be expressed as [10]

$$\hat{\sigma}_{\mathrm{LO}}(gg \to \phi_1\phi_2) = \int_{\hat{t}_-}^{\hat{t}_+} d\hat{t} \frac{G_F^2 \alpha_s^2(\mu)}{256(2\pi)^3} \left\{ |C_\triangle F_\triangle + C_\square F_\square|^2 + |C_\square G_\square|^2 \right\}. \tag{11}$$

The Mandelstam variables for the parton process are given by

$$\hat{s} = Q^2,$$

$$\hat{t} = -\frac{1}{2}\left[Q^2 - m_1^2 - m_2^2 - \sqrt{\lambda(Q^2, m_1^2, m_2^2)} \cos\theta \right],$$

$$\hat{u} = -\frac{1}{2}\left[Q^2 - m_1^2 - m_2^2 + \sqrt{\lambda(Q^2, m_1^2, m_2^2)} \cos\theta \right], \tag{12}$$

---

[2]Note that in the earlier Refs. [14, 16, 18] a factor of 1/2 is missing in the effective Lagrangians for the single pseudoscalar Higgs-boson coupling to gluons.

$$i\delta_{ab}\frac{\alpha_s}{3\pi v}g_t^H\left\{-g^{\mu\nu}(k_1\cdot k_2)+k_1^\nu k_2^\mu\right\}\left(1+\frac{11}{4}\frac{\alpha_s}{\pi}\right)$$

$$i\delta_{ab}\frac{\alpha_s}{2\pi v}g_t^A\epsilon^{\mu\nu\alpha\beta}k_{1\alpha}k_{2\beta}$$

$$-i\delta_{ab}\frac{\alpha_s}{3\pi v^2}g_t^{H_1}g_t^{H_2}\left\{-g^{\mu\nu}(k_1\cdot k_2)+k_1^\nu k_2^\mu\right\}\left(1+\frac{11}{4}\frac{\alpha_s}{\pi}\right)$$

$$i\delta_{ab}\frac{\alpha_s}{3\pi v^2}(g_t^A)^2\left\{-g^{\mu\nu}(k_1\cdot k_2)+k_1^\nu k_2^\mu\right\}\left(1+\frac{11}{4}\frac{\alpha_s}{\pi}\right)$$

$$-i\delta_{ab}\frac{\alpha_s}{2\pi v^2}g_t^H g_t^A\epsilon^{\mu\nu\alpha\beta}k_{1\alpha}k_{2\beta}$$

Figure 1: *Feynman rules for the effective interactions of Higgs bosons with gluons in the heavy-quark limit, including NLO corrections.*
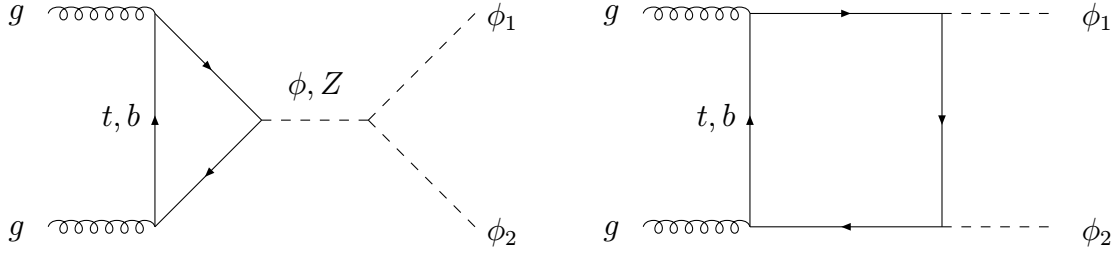
Figure 2: *Generic diagrams describing neutral Higgs-boson pair production in gluon–gluon collisions ($\phi, \phi_i = h, H, A$).*

where θ is the scattering angle in the partonic c.m. system with invariant mass Q, and

$$\lambda(x, y, z) = (x - y - z)^2 - 4yz. \tag{13}$$

The integration limits

$$\hat{t}_\pm = -\frac{1}{2}\left[Q^2 - m_1^2 - m_2^2 \mp \sqrt{\lambda(Q^2, m_1^2, m_2^2)}\right] \tag{14}$$

in Eq. (11) correspond to $\cos\theta = \pm 1$. The scale parameter μ is the renormalization scale. The complete dependence on the fermion masses is contained in the functions $F_\triangle$, $F_\square$, and $G_\square$. The full expressions of the form factors $F_\triangle$, $F_\square$, $G_\square$, including the exact dependence on the fermion masses, can be found in Ref. [10].

The couplings $C_\triangle$ and $C_\square$ and the form factors $F_\triangle, F_\square, G_\square$ in the heavy-quark limit are given by:

(i) SM:

$$
\begin{aligned}
C_\triangle &= \lambda_{HHH}\frac{M_Z^2}{\hat{s} - M_H^2 + iM_H\Gamma_H}, \qquad C_\square = 1, \\
F_\triangle &\rightarrow \frac{2}{3}, \qquad F_\square \rightarrow -\frac{2}{3}, \\
G_\square &\rightarrow 0,
\end{aligned}
\tag{15}
$$

with the trilinear coupling $\lambda_{HHH} = 3M_H^2/M_Z^2$.

(ii) MSSM:

The couplings for the processes $gg \rightarrow \phi_1\phi_2$ are generically defined as ($\phi, \phi_i = h, H, A$)

$$C_\triangle^\phi = \lambda_{\phi_1\phi_2\phi}\frac{M_Z^2}{\hat{s} - M_\phi^2 + iM_\phi\Gamma_\phi}g_t^\phi, \qquad C_\square = g_t^{\phi_1}g_t^{\phi_2}, \tag{16}$$

where ϕ denotes the Higgs particles of the s-channel contributions. The trilinear couplings $\lambda_{\phi_1\phi_2\phi}$ and the normalized Yukawa couplings g_t^ϕ can be found in Ref. [10]. The individual expressions in the heavy-quark limit can be summarized as:

7

$\phi_1\phi_2 = hh, hH, HH$:

$$
\begin{aligned}
C_\triangle &= C_\triangle^h + C_\triangle^H, \\
F_\triangle &\to \frac{2}{3}, & F_\square &\to -\frac{2}{3}, \\
G_\square &\to 0.
\end{aligned}
\tag{17}
$$

$\phi_1\phi_2 = hA, HA$:

$$
\begin{aligned}
C_\triangle &= C_\triangle^A + C_\triangle^Z, & C_\triangle^Z &= \lambda_{ZAh,ZAH}\, \frac{M_Z^2}{\hat{s} - M_Z^2 + iM_Z\Gamma_Z}\, a_t, \\
F_\triangle^A &\to 1, & F_\triangle^Z &\to \frac{\hat{s} - M_Z^2}{M_Z^2 \hat{s}}(M_{h,H}^2 - M_A^2), & F_\square &\to -1, \\
G_\square &\to 0,
\end{aligned}
\tag{18}
$$

where $a_t = 1$ denotes the axial charge of the top quark.

$\phi_1\phi_2 = AA$:

$$
\begin{aligned}
C_\triangle &= C_\triangle^h + C_\triangle^H, \\
F_\triangle &\to \frac{2}{3}, & F_\square &\to \frac{2}{3}, \\
G_\square &\to 0.
\end{aligned}
\tag{19}
$$

It should be noted that owing to the Ward identities for the Zgg vertex only the pseudoscalar Goldstone component of the Z bosons contributes to $F_\triangle^Z$ in the case of hA and HA production in the heavy-quark limit. The anomaly contributions of the top and bottom quarks cancel.

The QCD corrections consist of two-loop virtual corrections, generated by gluon exchange between the quark lines and/or external gluons, and one-loop real corrections with an additional gluon or light quark in the final state. We have evaluated the QCD corrections in the heavy-quark limit by means of two different methods: (i) using the effective couplings based on the low-energy theorems, as presented in the previous section, and (ii) explicitly expanding all relevant one- and two-loop diagrams in the inverse heavy-quark mass. In the following we shall describe the details of both approaches.

3.2   Low-energy theorems

We are now in a position to compute the NLO corrections to Higgs-boson pair production. Typical effective diagrams contributing to the virtual and real corrections are presented in Fig. 3. Adopting the Feynman rules of Fig. 1 for the effective interactions, the calculation has been carried out in dimensional regularization with $n = 4 - 2\epsilon$ dimensions. The strong coupling has been renormalized in the $\overline{\text{MS}}$ scheme including five light-quark flavours, i.e. decoupling the top quark in the running of α_s. After summing the virtual and real
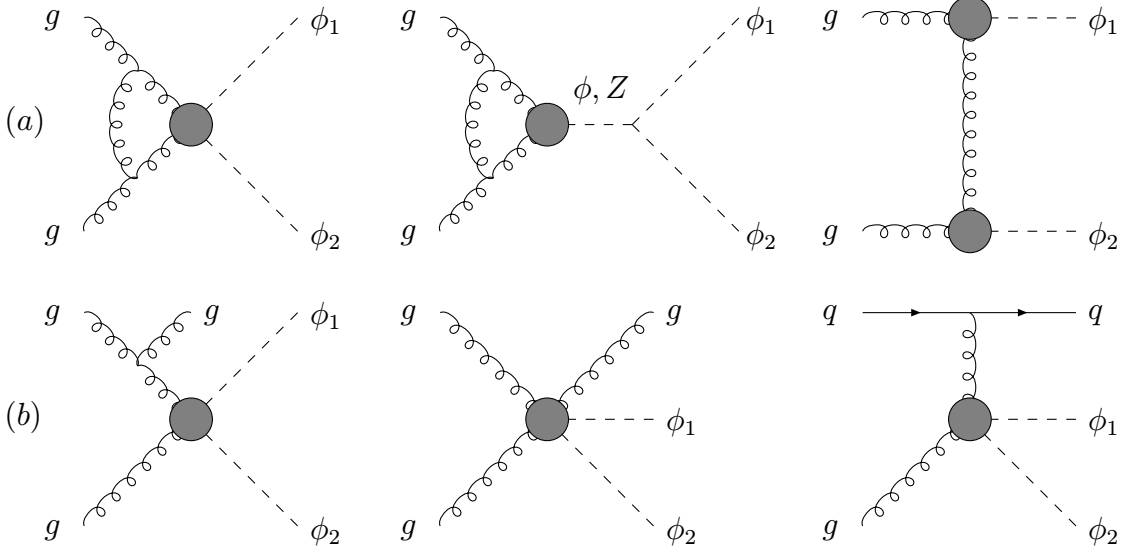
Figure 3: *Typical effective diagrams contributing to the (a) virtual and (b) real corrections to neutral Higgs-boson pair production.*

corrections the infrared singularities cancel. However, collinear initial-state singularities are left over in the partonic cross sections. Those divergences have been absorbed into the NLO parton densities, defined in the $\overline{\text{MS}}$ scheme with five light-quark flavours. We end up with finite results, which can be cast into the form

$$\sigma_{\text{NLO}}(pp \to \phi_1\phi_2 + X) = \sigma_{\text{LO}} + \Delta\sigma_{\text{virt}} + \Delta\sigma_{gg} + \Delta\sigma_{gq} + \Delta\sigma_{q\bar{q}}, \tag{20}$$

with the individual contributions

$$
\begin{aligned}
\sigma_{\text{LO}} &= \int_{\tau_0}^1 d\tau \, \frac{d\mathcal{L}^{gg}}{d\tau} \, \hat{\sigma}_{\text{LO}}(Q^2 = \tau s), \\
\Delta\sigma_{\text{virt}} &= \frac{\alpha_s(\mu)}{\pi} \int_{\tau_0}^1 d\tau \, \frac{d\mathcal{L}^{gg}}{d\tau} \, \hat{\sigma}_{\text{LO}}(Q^2 = \tau s) \, C, \\
\Delta\sigma_{gg} &= \frac{\alpha_s(\mu)}{\pi} \int_{\tau_0}^1 d\tau \, \frac{d\mathcal{L}^{gg}}{d\tau} \int_{\tau_0/\tau}^1 \frac{dz}{z} \, \hat{\sigma}_{\text{LO}}(Q^2 = z\tau s) \left\{ -zP_{gg}(z) \log\frac{M^2}{\tau s} \right. \\
&\qquad\qquad \left. -\frac{11}{2}(1-z)^3 + 6[1 + z^4 + (1-z)^4] \left(\frac{\log(1-z)}{1-z} \right)_+ \right\}, \\
\Delta\sigma_{gq} &= \frac{\alpha_s(\mu)}{\pi} \int_{\tau_0}^1 d\tau \sum_{q,\bar{q}} \frac{d\mathcal{L}^{gq}}{d\tau} \int_{\tau_0/\tau}^1 \frac{dz}{z} \, \hat{\sigma}_{\text{LO}}(Q^2 = z\tau s) \left\{ -\frac{z}{2}P_{gq}(z) \log\frac{M^2}{\tau s(1-z)^2} \right. \\
&\qquad\qquad\qquad\qquad \left. +\frac{2}{3}z^2 - (1-z)^2 \right\}, \\
\Delta\sigma_{q\bar{q}} &= \frac{\alpha_s(\mu)}{\pi} \int_{\tau_0}^1 d\tau \sum_q \frac{d\mathcal{L}^{q\bar{q}}}{d\tau} \int_{\tau_0/\tau}^1 \frac{dz}{z} \, \hat{\sigma}_{\text{LO}}(Q^2 = z\tau s) \, \frac{32}{27}(1-z)^3. \tag{21}
\end{aligned}
$$

9

The coefficient C for the virtual corrections reads

$$C = \pi^2 + c_1 + \frac{33 - 2N_F}{6} \log \frac{\mu^2}{Q^2}$$

$$+ \Re e \, \frac{\int_{\hat{t}_-}^{\hat{t}_+} d\hat{t} \left\{ c_2 \, C_\square (C_\triangle F_\triangle + C_\square F_\square) + c_3 \, \frac{p_T^2}{2\hat{t}\hat{u}} (Q^2 - m_1^2 - m_2^2) C_\square^2 G_\square \right\}}{\int_{\hat{t}_-}^{\hat{t}_+} d\hat{t} \left\{ |C_\triangle F_\triangle + C_\square F_\square|^2 + |C_\square G_\square|^2 \right\}}, \quad (22)$$

where

$$\tau_0 = \frac{(m_1 + m_2)^2}{s}, \qquad p_T^2 = \frac{(\hat{t} - m_1^2)(\hat{u} - m_1^2)}{Q^2} - m_1^2. \quad (23)$$

The objects $P_{gg}(z), P_{gq}(z)$ denote the Altarelli–Parisi splitting functions [20]:

$$P_{gg}(z) = 6 \left\{ \left(\frac{1}{1-z} \right)_+ + \frac{1}{z} - 2 + z(1-z) \right\} + \frac{33 - 2N_F}{6} \delta(1 - z),$$

$$P_{gq}(z) = \frac{4}{3} \frac{1 + (1-z)^2}{z}, \quad (24)$$

where $N_F = 5$ in our case. The factorization scale of the parton–parton luminosities $d\mathcal{L}^{ij}/d\tau$ is denoted by M. The coefficients c_i for the individual final-state Higgs bosons $\phi_1 \phi_2$ are given by

$$\phi_1 \phi_2 = hh, hH, HH : \qquad c_1 = \frac{11}{2}, \qquad c_2 = \frac{4}{9}, \qquad c_3 = -\frac{4}{9},$$

$$\phi_1 \phi_2 = hA, HA : \qquad c_1 = 6, \qquad c_2 = \frac{2}{3}, \qquad c_3 = \frac{2}{3} \frac{\hat{t} - \hat{u}}{Q^2 - m_1^2 - m_2^2},$$

$$\phi_1 \phi_2 = AA : \qquad c_1 = \frac{11}{2}, \qquad c_2 = -1, \qquad c_3 = -1. \quad (25)$$

In order to improve the validity of our results, we have inserted the full expressions for the form factors $F_\triangle, F_\square$ and $G_\square$ in Eqs. (11) and (22), i.e. including the exact dependence on the fermion masses. This procedure is reasonable since the QCD corrections are dominated by soft and collinear gluon radiation, which do not resolve the Higgs couplings to gluons, analogously to single-Higgs production via gluon fusion [12].

A few remarks on the s-channel Z-boson exchange in hA, HA production are in order. For the virtual corrections, the factorization of the NLO corrections into the LO form factors and a universal correction factor is exact for $m_t \to \infty$ and $m_b = 0$. This is due to the fact that only the pseudoscalar Goldstone component of the Z boson contributes as in LO, i.e. the QCD corrections coincide with the one to s-channel pseudoscalar Higgs-boson exchange. For the real corrections, the factorization is not exact, but the applied correction factor correctly includes the dominant contributions, which are caused by soft and collinear gluon radiation. Additional infrared- and collinear-finite contributions, e.g. originating from $Zggg$ box corrections in $gg \to g + Z^* \to g + hA, HA$ processes, are expected to be small, since they do not exhibit large contributions from soft and collinear gluon radiation. They are neglected in our analysis.

10

3.3 Explicit expansion of the gluon-fusion diagrams

We have derived the above results also by explicitly performing the heavy-mass expansion of the corresponding one- and two-loop Feynman diagrams. The amplitudes for the individual diagrams have been automatically generated using the package *FeynArts* [21]. The asymptotic expansion of the individual amplitudes in the heavy top-quark mass is carried out directly in the integrand, i.e. before the integration over the momentum space. We employ the general algorithm of Ref. [22] (see also Ref. [23] and references therein) for the asymptotic expansion of Feynman diagrams in dimensional regularization. This method expresses the coefficients of the expansion in terms of simpler diagrams. At the one-loop level, this procedure leads to simple one-loop vacuum integrals only. At the two-loop level, we get two-loop vacuum integrals and products of one-loop vacuum integrals and massless one-loop integrals with non-vanishing external momenta. The analytical calculation of all those integrals is straightforward when using the Feynman-parameter technique. Since the employed strategy leads to a very large number of terms in intermediate steps, and since each step is algorithmic, we have fully automatized the calculation in *Mathematica* [24]. In the following we sketch the single steps of the calculation and give the results for the basic integrals.

The general algorithm for the asymptotic expansion of any given Feynman graph Γ in the limit $M_i \to \infty$ for some internal masses M_i can easily be summarized. Denoting the corresponding Feynman amplitude by F_Γ and the corresponding integrand by I_Γ, the large-mass expansion reads

$$F_\Gamma \;=\; \int \left(\prod_l d^n q_l \right) I_\Gamma \quad \widetilde{M_i \to \infty} \quad \sum_\gamma \int \left(\prod_l d^n q_l \right) I_{\Gamma/\gamma} \, \mathcal{T}_{p_i^\gamma, m_i} I_\gamma, \qquad (26)$$

where q_l are the integration momenta. The sum on the r.h.s. runs over all subgraphs γ of Γ which contain all propagators with the heavy masses M_i and which are irreducible with respect to those lines of γ that carry light masses m_i. The integrand of the subgraph γ is denoted by I_γ. The reduced graph Γ/γ results from Γ upon shrinking γ to a point, and the integrand $I_{\Gamma/\gamma}$ is defined such that $I_\Gamma = I_\gamma I_{\Gamma/\gamma}$. The symbol $\mathcal{T}_{p_i^\gamma, m_i}$ represents an operator that replaces the integrand I_γ by its Taylor series in the expansion parameters p_i^γ and m_i, where p_i^γ are the external momenta of the subgraph γ. Therefore, Eq. (26) expresses the original integral F_Γ in terms of an infinite sum over simpler integrals. For any given power ξ^a, this sum contains only a finite number of terms that are non-vanishing in $(F_\Gamma|_{M_i \to \xi M_i})/\xi^a$ after the scaling limit $\xi \to \infty$ is taken. These terms can easily be determined by power counting. This general strategy for the heavy-mass expansion will become more transparent when we inspect in more detail the different types of graphs that are relevant in our case.

We start by considering the relevant one-loop integrals in the limit $m_t \to \infty$. They contain only top-quark propagators in the loop, both for the LO calculation and for the real NLO corrections. According to the algorithm (26), there is only one relevant subgraph γ, namely the subgraph γ_{loop} containing only the propagators of lines inside the loop. If Γ is irreducible, we have $\Gamma = \gamma_{\text{loop}}$. The Taylor-expansion operator $\mathcal{T}$ replaces

each propagator $P(q - p, m_t)$ by

$$P(q - p, m_t) = [(q - p)^2 - m_t^2]^{-1} = \sum_{l=0}^{\infty} (q^2 - m_t^2)^{-1-l} (2qp - p^2)^l, \qquad (27)$$

where q denotes the integration momentum, and p is any combination of external momenta. These replacements express each one-loop diagram by a sum of terms containing one-loop vacuum integrals

$$V^{(1)}_{\mu_1 \ldots \mu_R}(n_1; m_1) = \frac{(2\pi\mu)^{4-n}}{i\pi^2} \int d^n q \, \frac{q_{\mu_1} \cdots q_{\mu_R}}{(q^2 - m_1^2)^{n_1}}. \qquad (28)$$

The terms that are non-vanishing in the heavy-mass limit can be determined by simple power counting, since an explicit factor of m_t and the integration momentum q contribute to the scaling factor in m_t exactly in the same way. All non-vanishing vacuum tensor integrals (28) can be decomposed into terms that are products of metric tensors $g_{\mu\nu}$ and coefficient factors. The coefficients for the different covariants, which span the whole tensor, can be algebraically expressed in terms of scalar vacuum integrals. This algebraic reduction, which proceeds recursively in the tensor rank, is standard. The trick is to contract the equation that expresses the integral in terms of covariants with a set of some suitably chosen covariants. On the side of the integral, this leads to integrals that are already known; on the other side of this equation, one gets linear combinations for the tensor coefficients. The coefficients are obtained by inverting a system of such linear equations for the coefficients. For the case of one-loop tensor vacuum integrals, at most a single covariant structure contributes, namely the totally symmetric tensor built of metric tensors $g_{\mu\nu}$. Only scalar one-loop integrals, i.e. the ones of (28) with $R = 0$, have to be computed explicitly. A simple calculation yields

$$V^{(1)}(n_1; m_1) = (-1)^{n_1} (4\pi\mu^2)^{\frac{4-n}{2}} m^{n-2n_1} \frac{\Gamma\left(n_1 - \frac{n}{2}\right)}{\Gamma(n_1)}. \qquad (29)$$

At the two-loop level, there are two basically different types of diagrams. The first type contains two independent top-quark loops. Such diagrams do not lead to genuine two-loop integrals and can be treated like the one-loop diagrams above. Topologically those diagrams are represented by the third graph of Fig. 3. The second type of graphs is formed by the genuine two-loop diagrams. Each of those diagrams contains a closed top-quark loop and one, two, or three internal gluon lines. Typical box diagrams are shown in Fig. 4. For all such genuine two-loop diagrams there are two subgraphs γ that are relevant in the expansion (26) for $m_t \to \infty$. The first subgraph is the diagram γ_{loop} built of all lines inside the loops, the second is given by the closed top-quark loop.

First we consider the case $\gamma = \gamma_{\text{loop}}$. The Taylor expansion of the integrand $I_{\gamma_{\text{loop}}}$ involves the consistent expansion of each propagator about the external momenta of the process. This means that each propagator $P(q - p, m)$ is replaced by

$$P(q - p, m) = [(q - p)^2 - m^2]^{-1} = \sum_{l=0}^{\infty} (q^2 - m^2)^{-1-l} (2qp - p^2)^l, \qquad m = 0, m_t, \quad (30)$$
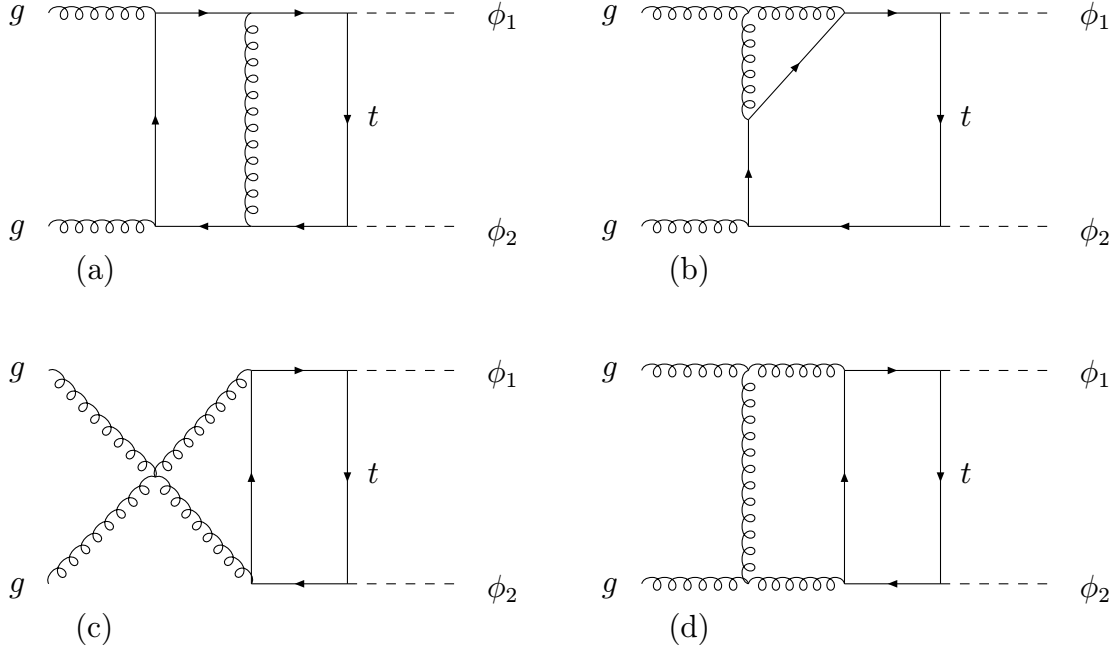
12

Figure 4: *Typical two-loop box diagrams with one, two, or three internal gluons.*

where q is a linear combination of the two integration momenta q_1 and q_2, and p consists of external momenta p_i. This replacement leads to two-loop vacuum integrals of the general form

$$
V^{(2)}_{\mu_1\ldots\mu_R;\nu_1\ldots\nu_S}(n_1,n_2,n_3;m_1,m_2,m_3)
$$
$$
= \frac{(2\pi\mu)^{4-n}}{i\pi^2}\int d^n q_1\,\frac{(2\pi\mu)^{4-n}}{i\pi^2}\int d^n q_2\,\frac{q_{1,\mu_1}\cdots q_{1,\mu_R}\,q_{2,\nu_1}\cdots q_{2,\nu_S}}{(q_1^2-m_1^2)^{n_1}(q_2^2-m_2^2)^{n_2}[(q_1+q_2)^2-m_3^2]^{n_3}},\quad (31)
$$

with the actual mass insertions $m_1 = 0$ and $m_2 = m_3 = m_t$. In the power counting, which determines the non-vanishing terms for $m_t \to \infty$, factors of the integration momenta q_1 and q_2 contribute in the same way as explicit factors of m_t. The algebraic reduction of two-loop tensor vacuum integrals proceeds along the same lines as described for the one-loop case above. The only difference is that tensors need not be totally symmetric beyond one loop. Finally, we are left with the scalar integral ($R = S = 0$), which can be easily calculated,

$$
V^{(2)}(n_1,n_2,n_3;0,m,m) = (-1)^{n_1+n_2+n_3}(4\pi\mu^2)^{4-n}(m^2)^{n-n_1-n_2-n_3}
$$
$$
\times\,\frac{\Gamma(n_1+n_2+n_3-n)\Gamma\left(\frac{n}{2}-n_1\right)\Gamma\left(n_1+n_2-\frac{n}{2}\right)\Gamma\left(n_1+n_3-\frac{n}{2}\right)}{\Gamma\left(\frac{n}{2}\right)\Gamma(n_2)\Gamma(n_3)\Gamma(2n_1+n_2+n_3-n)}.\quad (32)
$$

Now we identify the subgraph γ with the top-quark loop. In this case the Taylor expansion in the integrand I_γ concerns the momenta that are external with respect to the

13

top-quark loop. Thus, all top-quark propagators $P(q_2 - p, m_t)$ are replaced by

$$P(q_2 - p, m_t) = [(q_2 - p)^2 - m_t^2]^{-1} = \sum_{l=0}^{\infty} (q_2^2 - m_t^2)^{-1-l} (2q_2 p - p^2)^l, \qquad (33)$$

where q_2 is the loop momentum running through the top-quark loop. Note that p includes all external momenta of the process as well as the loop momentum q_1 running through the internal gluon lines. The integration over q_2 leads to one-loop vacuum integrals of the form (28), the calculation of which is described above. The integration over q_1 involves only massless propagators to the first power. Since the q_1 integration does not involve any m_t-terms, it does not affect the power counting in m_t at all. For one-gluon exchange the integral over q_1 is a massless tadpole, which vanishes in dimensional regularization. For two-gluon and three-gluon exchange the q_1 integration leads to the one-loop tensor integrals

$$B_{\mu_1 \ldots \mu_R}(p) = \frac{(2\pi\mu)^{4-n}}{i\pi^2} \int d^n q_1 \, \frac{q_{1,\mu_1} \cdots q_{1,\mu_R}}{q_1^2 (q_1 + p)^2},$$

$$C_{\mu_1 \ldots \mu_R}(p_1, p_2) = \frac{(2\pi\mu)^{4-n}}{i\pi^2} \int d^n q_1 \, \frac{q_{1,\mu_1} \cdots q_{1,\mu_R}}{q_1^2 (q_1 + p_1)^2 (q_1 + p_2)^2}. \qquad (34)$$

The tensor integrals can again be recursively reduced to the corresponding scalar integrals in a fully algebraic manner. The relevant scalar integrals can be easily calculated and are given by

$$B(p)\big|_{p^2 \neq 0} = \left(\frac{4\pi\mu^2}{-p^2 - i0} \right)^{\frac{4-n}{2}} \frac{\Gamma\left(2 - \frac{n}{2}\right) \Gamma\left(\frac{n}{2} - 1\right)^2}{\Gamma(n-2)},$$

$$C(p_1, p_2)\big|_{p_1^2 = p_2^2 = 0, \, p^2 = (p_1 - p_2)^2 \neq 0} = \frac{1}{p^2} \left(\frac{4\pi\mu^2}{-p^2 - i0} \right)^{\frac{4-n}{2}} \frac{\Gamma\left(3 - \frac{n}{2}\right) \Gamma\left(\frac{n}{2} - 2\right)^2}{\Gamma(n-3)}. \qquad (35)$$

For $p^2 = 0$ the integrals are zero in dimensional regularization. The case $B(p)$ with $p^2 = 0$ occurs, for instance, in graphs like Fig. 4b. Therefore, we find that the contribution in the expansion (26) for which γ is the top-quark loop is only non-vanishing in diagrams like Figs. 4c and d, where both external gluons are attached to the internal gluon lines.

A few more "physical" remarks on the formally described algorithm for the asymptotic expansion seem to be in order. The different contributions to a given Feynman graph that are associated with the subgraphs γ in the expansion (26) are directly related to the effective diagrams in the approach of the low-energy theorem described above. Shrinking the subgraph γ to a point leads to the corresponding effective diagram, where the point arising from γ is the point-like interaction of the effective Lagrangian. A non-vanishing contribution of a subgraph $\gamma \neq \gamma_{\text{loop}}$ requires that at least one external momentum p_i passes through a massless propagator; otherwise the loop integral involving the massless propagators is zero. In other words, it is necessary that there exists a cut through

the diagram that passes exclusively massless lines. Therefore, only diagrams with such a "massless cut" can lead to contributions to effective diagrams in which an effective coupling appears in loops. But all diagrams in general contribute to tree-like effective diagrams, which result from shrinking the complete loop part γ_{loop} to a point.

Finally, we mention that γ_5, which appears in the case of pseudoscalar Higgs bosons, is treated according to the prescription of 't Hooft and Veltman [25]. Technically we substitute γ_5 by $i\epsilon^{\mu_1\mu_2\mu_3\mu_4}\gamma_{\mu_1}\gamma_{\mu_2}\gamma_{\mu_3}\gamma_{\mu_4}/4!$ before the evaluation of the Dirac trace so that the actual trace calculation can be carried out for usual n-dimensional Dirac matrices. The correct projection of the trace result on the physical four-dimensional space is achieved upon the contraction with the four-dimensional ϵ-tensor. In this approach, all loop integrations can be carried out before the contraction with ϵ, i.e. n-dimensional momenta can be used. Note, however, that the contraction with ϵ necessarily occurs before the integration over the phase space of the radiated parton in the real corrections, i.e. one has to take care of the four-dimensionality of ϵ there. Moreover, an additional spurious counter term has to be added to the $At\bar{t}$ vertex (see also [14, 18]).
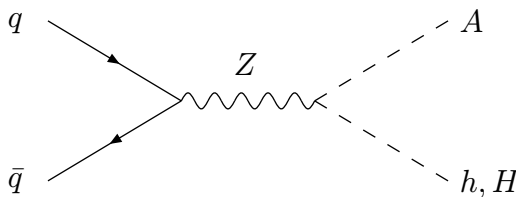
3.4 Drell–Yan-like processes

Figure 5: *Diagram contributing to $q\bar{q} \to Ah, AH$ at lowest order.*

Pairs of scalar and pseudoscalar Higgs bosons can also be produced in $q\bar{q}$ collisons via s-channel Z-boson exchange, see Fig. 5. At LO the partonic cross sections are given by

$$\hat{\sigma}_{\text{LO}}(q\bar{q} \to Ah, AH) = \lambda_{ZAh,ZAH}^2 \frac{G_F^2 M_Z^4}{288\pi}(v_q^2 + a_q^2)\frac{\lambda(Q^2, M_A^2, M_{h,H}^2)^{\frac{3}{2}}}{(Q^2)^2(Q^2 - M_Z^2)^2},\qquad(36)$$

where Q^2 denotes the partonic c.m. energy squared, and $v_q = 2I_{3q} - 4e_q \sin^2\theta_W$, $a_q = 2I_{3q}$ are the vectorial and axial charges of the initial-state quarks. The QCD corrections coincide analytically with the QCD corrections to the Drell–Yan process $q\bar{q} \to Z^*$, if squarks and gluinos are heavy, so that their contributions can be neglected. Thus the NLO cross section can be expressed as:

$$\sigma_{\text{NLO}}(pp \to Ah, AH + X) = \sigma_{\text{LO}} + \Delta\sigma_{q\bar{q}} + \Delta\sigma_{qg},$$
$$\sigma_{\text{LO}} = \int_{\tau_0}^1 d\tau \sum_q \frac{d\mathcal{L}^{q\bar{q}}}{d\tau}\hat{\sigma}_{\text{LO}}(Q^2 = \tau s),$$

15

$$\Delta\sigma_{q\bar{q}} = \frac{\alpha_s(\mu)}{\pi}\int_{\tau_0}^1 d\tau \sum_q \frac{d\mathcal{L}^{q\bar{q}}}{d\tau}\int_{\tau_0/\tau}^1 dz \ \hat{\sigma}_{\rm LO}(Q^2=\tau zs)\,\omega_{q\bar{q}}(z),$$

$$\Delta\sigma_{qg} = \frac{\alpha_s(\mu)}{\pi}\int_{\tau_0}^1 d\tau \sum_{q,\bar{q}} \frac{d\mathcal{L}^{qg}}{d\tau}\int_{\tau_0/\tau}^1 dz \ \hat{\sigma}_{\rm LO}(Q^2=\tau zs)\,\omega_{qg}(z), \quad (37)$$

with the coefficient functions [26]

$$\omega_{q\bar{q}}(z) = -P_{qq}(z)\log\frac{M^2}{\tau s} + \frac{4}{3}\left\{2[\zeta_2-2]\delta(1-z)+4\left(\frac{\log(1-z)}{1-z}\right)_+\right.$$
$$\left. -2(1+z)\log(1-z)\right\},$$

$$\omega_{qg}(z) = -\frac{1}{2}P_{qg}(z)\log\left(\frac{M^2}{(1-z)^2\tau s}\right) + \frac{1}{8}\left\{1+6z-7z^2\right\}. \quad (38)$$

The Altarelli–Parisi splitting functions $P_{q\bar{q}}$ and P_{qg} are given by [20]

$$P_{qq}(z) = \frac{4}{3}\left\{2\left(\frac{1}{1-z}\right)_+ -1-z+\frac{3}{2}\delta(1-z)\right\},$$

$$P_{qg}(z) = \frac{1}{2}\left\{z^2+(1-z)^2\right\}. \quad (39)$$

4 Results

4.1 Standard Model

The analysis for SM Higgs-boson pair production has been carried out for the LHC c.m. energy $\sqrt{s} = 14$ TeV. The top-quark and bottom-quark masses have been chosen as $m_t = 175$ GeV and $m_b = 5$ GeV. We have adopted the CTEQ4L and CTEQ4M [27] parton densities for the LO and NLO cross sections, respectively, corresponding to the QCD parameters $\Lambda_5^{\rm LO} = 181$ MeV and $\Lambda_5^{\overline{\rm MS}} = 202$ MeV. Since our results have been obtained in the heavy-quark limit, they can be expected to be reliable for $M_H \lesssim 200$ GeV, based on the experience from single-Higgs production via gluon fusion.

In order to investigate the size of the QCD corrections, we define the K factor $K = \sigma_{\rm NLO}/\sigma_{\rm LO}$ as the ratio of the NLO and LO cross sections, where the parton densities and the strong coupling α_s are taken at NLO and LO, respectively. The K factor for SM-Higgs pair production is presented in Fig. 6 as a function of the Higgs mass M_H and shows little variation with M_H. It ranges between about 1.9 and 2.0, thus enhancing the LO cross section significantly. Moreover, the broken lines of Fig. 6 show the contributions of the individual terms of Eq. (20). It can be clearly inferred that analogously to the case of single-Higgs production the (infrared-regularized) virtual and real corrections originating from gg intial states dominate the QCD corrections, while the gq and $q\bar{q}$ initial states do not exceed about 5% in total. We note that the values shown for $K_{\rm virt}$, K_{gg}, K_{gq}, and K_{qq} do not exactly add up to $K_{\rm tot}-1$, since the individual contributions are obtained by
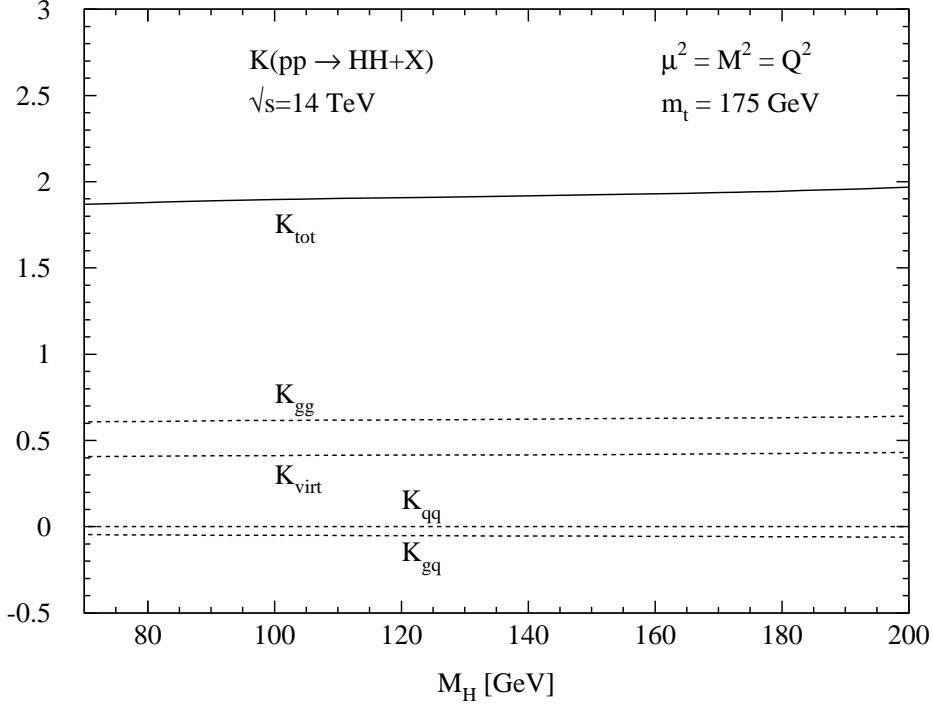
16

Figure 6: *K factors of the QCD-corrected gluon-fusion SM cross section $\sigma(pp \to HH + X)$ at the LHC with c.m. energy $\sqrt{s} = 14$ TeV. The dashed lines show the individual contributions of the four terms of the QCD corrections given in Eq. (20).*
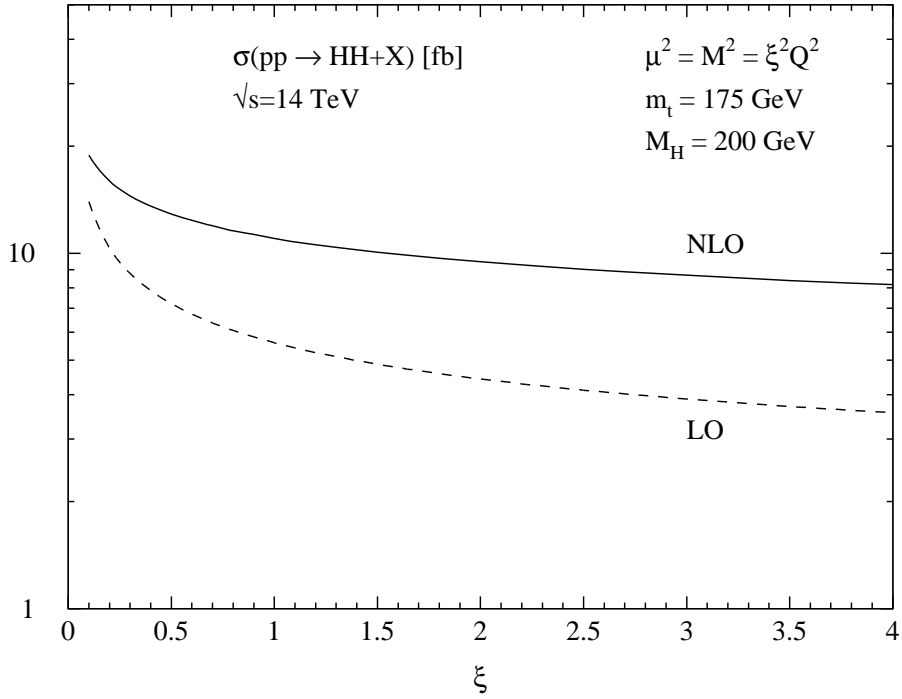

Figure 7: *The renormalization and factorization scale dependence of the SM-Higgs pair-production cross section at LO and NLO for a Higgs mass $M_H = 200$ GeV.*

17

taking NLO parton densities and the strong coupling in the NLO cross sections, but LO quantities in the LO cross sections consistently.

In order to investigate the reliability of our results, the residual dependence of the cross section on the renormalization and factorization scales is shown in Fig. 7 for a Higgs mass of $M_H = 200$ GeV at LO and NLO. The scale dependence significantly decreases compared with the LO result by including the QCD corrections. However, the still monotonic decrease of the NLO cross section with increasing scales signals the need for further improvements. Nevertheless, the theoretical uncertainty of the NLO result can be estimated to about 20% from the residual scale dependence.

The final results for the total Higgs pair-production cross sections at LO and NLO are presented in Fig. 8 as a function of the Higgs mass M_H. We recall that the full mass dependence of the LO form factors is included in all numerical evaluations, i.e. only the relative NLO correction is treated in the heavy-quark limit, in order to increase the validity of our results. For $M_H \lesssim 200$ GeV the cross section exceeds 10 fb, leading to more than about 3000 events at the LHC, once the anticipated integrated luminosity $\int \mathcal{L} dt = 3 \times 10^5$ pb^{-1} is reached[3]. The typical signatures for Higgs-boson pair production are $b\bar{b}b\bar{b}$ and $b\bar{b}\tau^+\tau^-$ final states for $M_H \lesssim 140$ GeV. For $M_H \gtrsim 160$ GeV, the Higgs-boson pairs decay predominantly into four vector bosons.

Finally, we present the sensitivity of the SM-Higgs pair-production cross section to the trilinear Higgs coupling in Fig. 9, which shows the ratio of the total cross section with a non-standard trilinear coupling λ and the SM one as a function of the trilinear coupling, varying in units of the SM coupling. The cross section becomes significantly larger for smaller trilinear couplings, so that this process may serve as a possibility to measure this coupling and test the SM Higgs sector, if the signal can be extracted from the QCD background.

The trilinear Higgs coupling can potentially be measured at high-energy e^+e^- colliders [28]. Since the rate for multiple Higgs-boson production at e^+e^- colliders is small, high luminosities are required for a sufficient number of events in order to probe this coupling. However, the backgrounds will be well under control.

4.2   Minimal supersymmetric extension

Promising MSSM-Higgs pair-production processes at the LHC are hh, hH, HH, hA and HA production with sizeable ranges in the parameter space where the cross sections exceed 10 fb [10]. The $gg \to hh$ process can be used to cover a part of the MSSM parameter space for small tgβ via its decay modes into $b\bar{b}\gamma\gamma$ final states [29] in the region where this process is dominated by resonant $gg \to H \to hh$ production. Since our calculation is expected to be valid for small values of tgβ (where the b-quark contribution can be neglected) and Higgs masses below the $t\bar{t}$ threshold, it may be assumed to reliably approximate the cross sections of light-scalar-Higgs pair-production in particular. Generally, in the MSSM, we expect our results to be valid for $M_A \lesssim 200$ GeV, while for larger pseudoscalar masses at

---

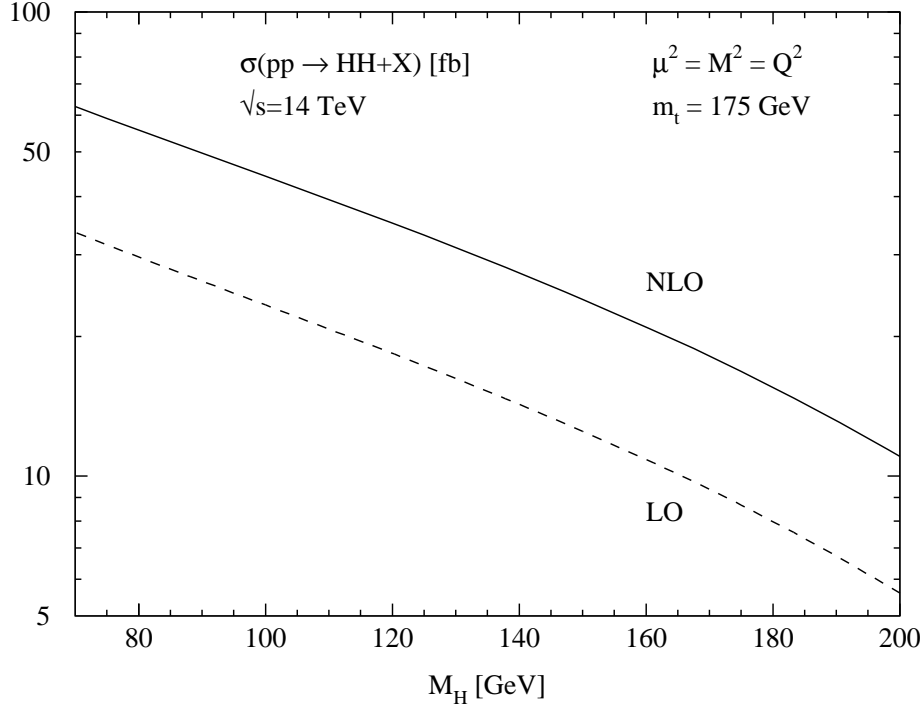[3]The cross section at the Tevatron is less than 0.2 fb for $\sqrt{s} = 2$ TeV.

Figure 8: *SM prediction of the Higgs-boson pair-production cross section at LO and NLO as a function of the Higgs mass M_H.*
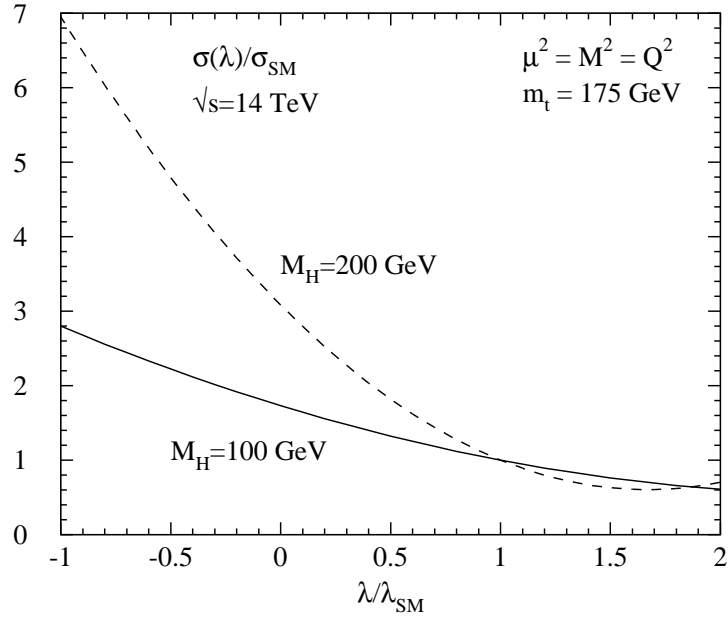

Figure 9: *Ratio of the Higgs-boson pair-production cross section at NLO with a non-standard trilinear coupling λ and the SM cross section as a function of the trilinear coupling in units of the SM one.*

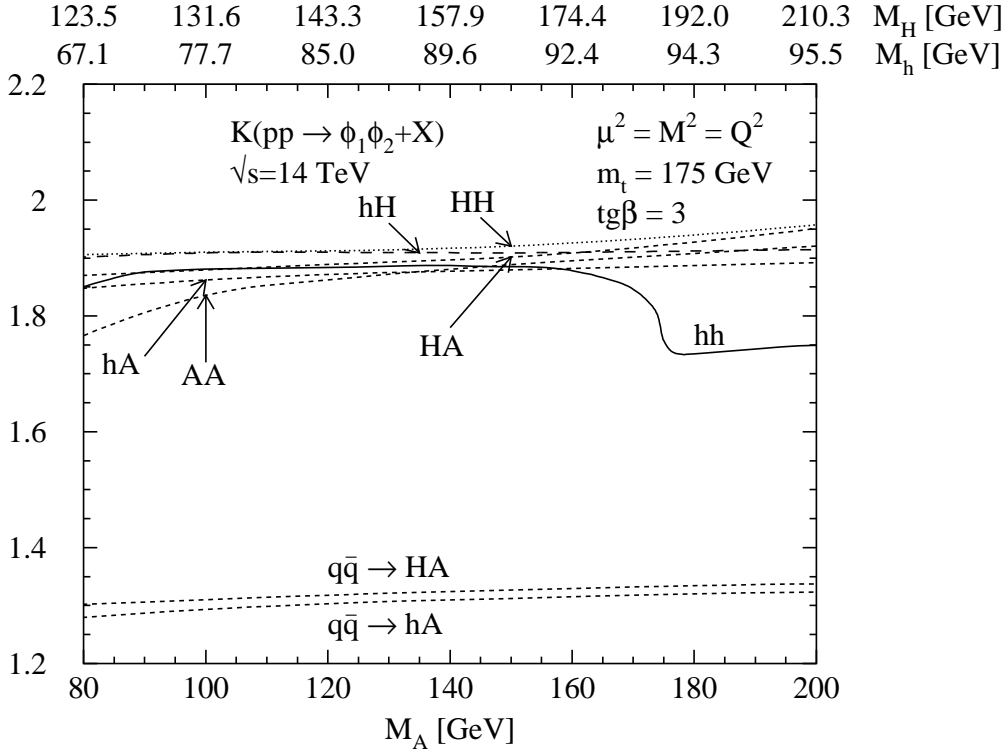| 123.5	131.6	143.3	157.9	174.4	192.0	210.3	M_H [GeV]
67.1	77.7	85.0	89.6	92.4	94.3	95.5	M_h [GeV]

Figure 10: *K factors of the QCD-corrected gluon-fusion and Drell–Yan like cross sections* $\sigma(pp \to \phi_1\phi_2 + X)$ *at the LHC with c.m. energy* $\sqrt{s} = 14$ *TeV.*

least the heavy s-channel Higgs particles become too heavy with respect to the top-quark mass.

In our analysis we have included the MSSM Higgs masses and couplings at the two-loop level in the effective-potential approach [5]. Moreover, we have included all available higher-order corrections to the total MSSM Higgs decay widths [30], which appear in the s-channel Higgs propagators of the triangular loop contributions.

The K factors for all Higgs-boson pair-production processes for $\text{tg}\beta = 3$ are presented in Fig. 10 as a function of the pseudoscalar Higgs mass M_A. The numbers at the top are the corresponding values of the Higgs masses M_h and M_H. The total K factors increase the Drell–Yan like cross sections by about 30% and the gg production cross sections by about 60–100%, thus signalling the importance of the QCD corrections. These are dominated by soft and collinear gluon radiation from gg and $q\bar{q}$ initial states, similar to the SM case discussed above in detail. The sharp decrease of the K factor for $gg \to hh$ at $M_A \sim 175$ GeV originates from the resonance contribution $gg \to H \to hh$, which is kinematically forbidden below this mass and allowed above. The K factor of resonant single-Higgs production is smaller than the one of continuum hh production.

In spite of the large size of the NLO contributions, the scale dependence significantly decreases as can be inferred from Fig. 11, which presents the scale dependence of the cross section $\sigma(pp \to hh + X)$ at LO and NLO for a light-scalar-Higgs mass $M_h = 95.5$ GeV, corresponding to $M_A = 200$ GeV. Thus, the QCD-corrected results turn out to be reliable
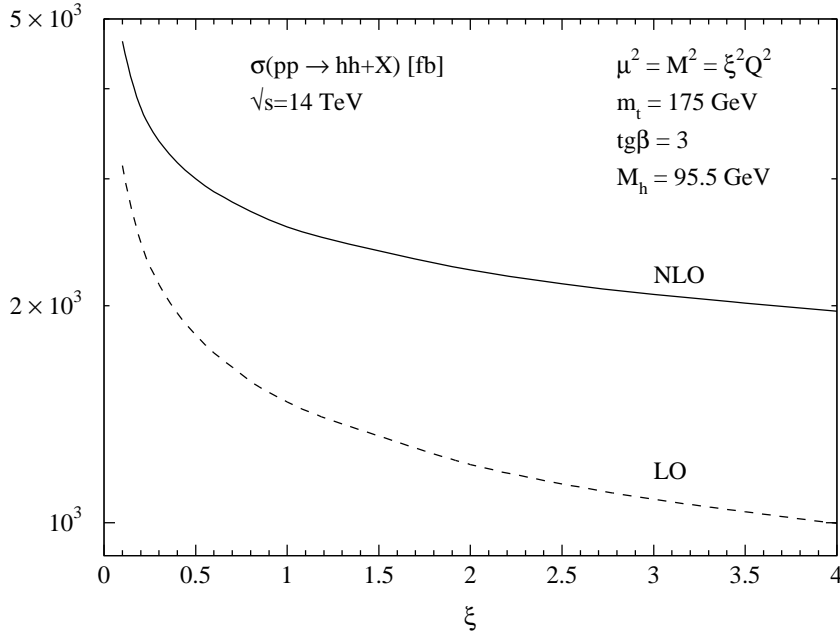
20

Figure 11: *The renormalization and factorization scale dependence of the Higgs pair-production cross section $\sigma(pp \to hh + X)$ at LO and NLO for $tg\beta = 3$ and a Higgs mass $M_h = 95.5$ GeV ($M_A = 200$ GeV).*
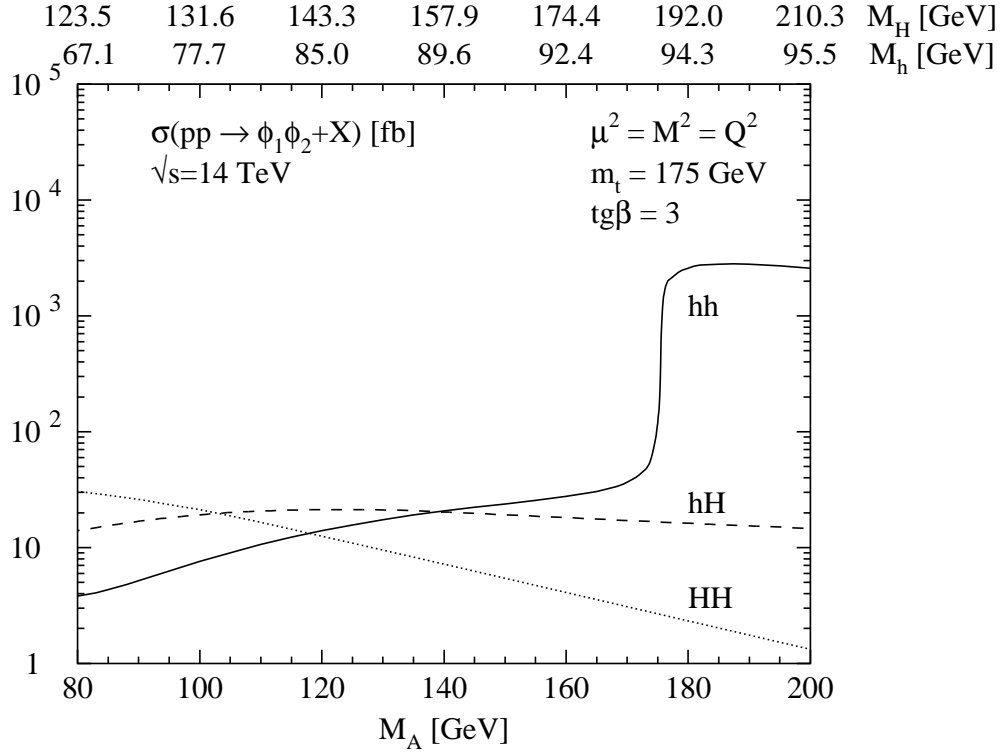

Figure 12: *Scalar Higgs-boson pair-production cross sections $\sigma(pp \to hh, hH, HH + X)$ at NLO as functions of the pseudoscalar Higgs mass M_A for $tg\beta = 3$.*

within about $\pm 20\%$. The total NLO cross sections for the processes $gg \to hh$, hH, HH are presented in Fig. 12 as a function of the pseudoscalar Higgs mass M_A. The sharp increase of the hh cross section at $M_A \sim 175$ GeV is due to the fact that the resonant $gg \to H \to hh$ process opens up above this mass value, while it is kinematically forbidden below. There are sizeable regions where the cross sections exceed a level of 10 fb. This is in contrast to AA production, the cross section of which is smaller than 1 fb in the considered parameter space.

The total cross sections for the processes $pp \to hA$, HA and their individual contributions from the gg and $q\bar{q}$ initiated processes are presented in Fig. 13 as a function of the pseudoscalar mass M_A for $tg\beta = 3$. While for HA-pair production gluon fusion $gg \to HA$ is always suppressed against the Drell–Yan like process $q\bar{q} \to HA$, both corresponding processes are competitive for the light scalar Higgs particle h. Especially for smaller masses M_A the total cross sections for $pp \to hA$, HA exceed 10 fb and thus potentially provide the possibility to detect these processes. Note, however, that only the gluon-fusion processes are sensitive to the trilinear Higgs couplings.

Finally, it should be noted, that in all neutral Higgs-pair processes the residual theoretical uncertainties reduce to a level of 20% after including the QCD corrections.

The corresponding NLO cross section for hh production at the Tevatron with c.m. energy $\sqrt{s} = 2$ TeV is presented in Fig. 14 as a function of the pseudoscalar mass M_A. For $M_A \gtrsim 175$ GeV it exceeds 10 fb, since the resonant $gg \to H \to hh$ is kinematically possible and dominant in this mass region. The signatures of this process are $b\bar{b}b\bar{b}$ and $b\bar{b}\tau^+\tau^-$ final states.

Trilinear MSSM Higgs couplings can be measured at high energy e^+e^- colliders [31], if sufficient numbers of signal events for Higgs pair production will be produced. At the necessary high luminosities background processes do not cause any problem.

5   Conclusions

We have presented a complete calculation of the two-loop QCD corrections to neutral-Higgs pair production at the LHC via gluon fusion in the limit of a heavy top quark. This approximation is at least reliable if the invariant mass of the produced Higgs-boson pair is below the tt threshold of the mediating top-quark loops. We have analyzed the results within the SM and the MSSM and found large increases of the cross sections by about 60–100%. The QCD corrections to the associated production processes $q\bar{q} \to hA$, HA coincide with those to the Drell–Yan process $q\bar{q} \to Z^*$, thus increasing the cross sections by about 30%. The QCD corrections stabilize the theoretical predictions compared with the LO results, which exhibit large theoretical uncertainties. After including the QCD corrections, the remaining theoretical uncertainties are reduced to a level of about 20%.

Except for AA-pair production, all Higgs-pair production cross sections of the SM and the MSSM exceed 10 fb at LHC energies in certain regions of the parameter spaces. As soon as the $H \to hh$ channel opens, the cross section for $pp \to hh + X$ reaches even 10^3 fb at the LHC and is still larger than 10 fb at the Tevatron for $tg\beta = 3$.
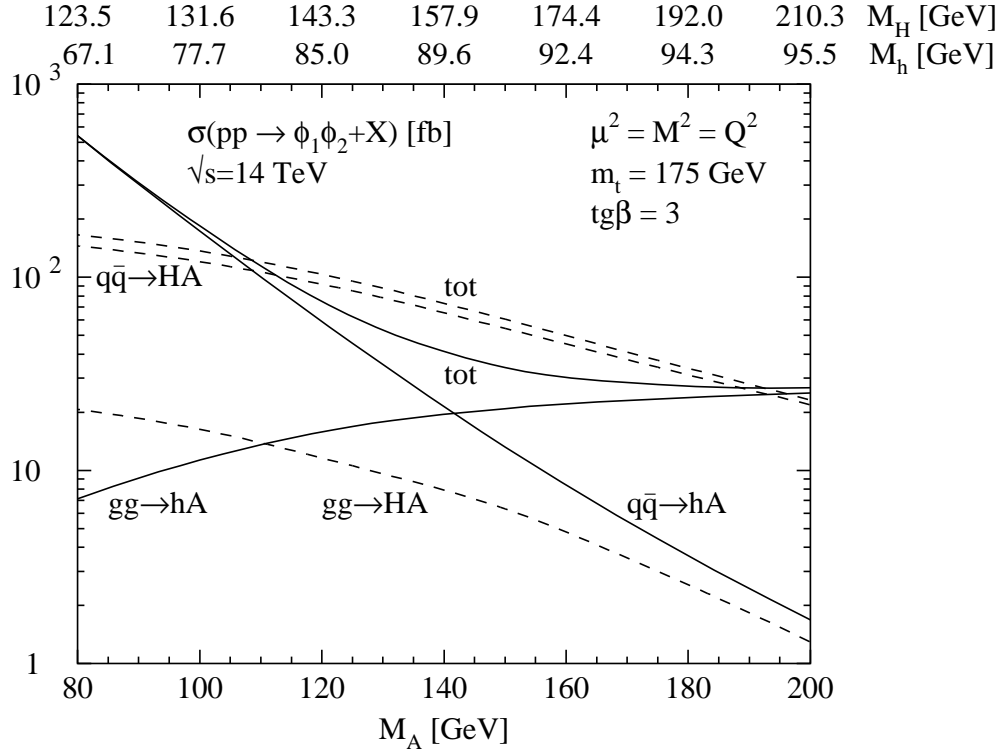
Figure 13: *Scalar and pseudoscalar Higgs-boson pair-production cross sections $\sigma(pp \to hA, HA + X)$ at NLO as functions of the pseudoscalar Higgs mass M_A for $tg\beta = 3$ and their individual contributions from gg and $q\bar{q}$ collisions. The full lines correspond to hA and the broken ones to HA production.*
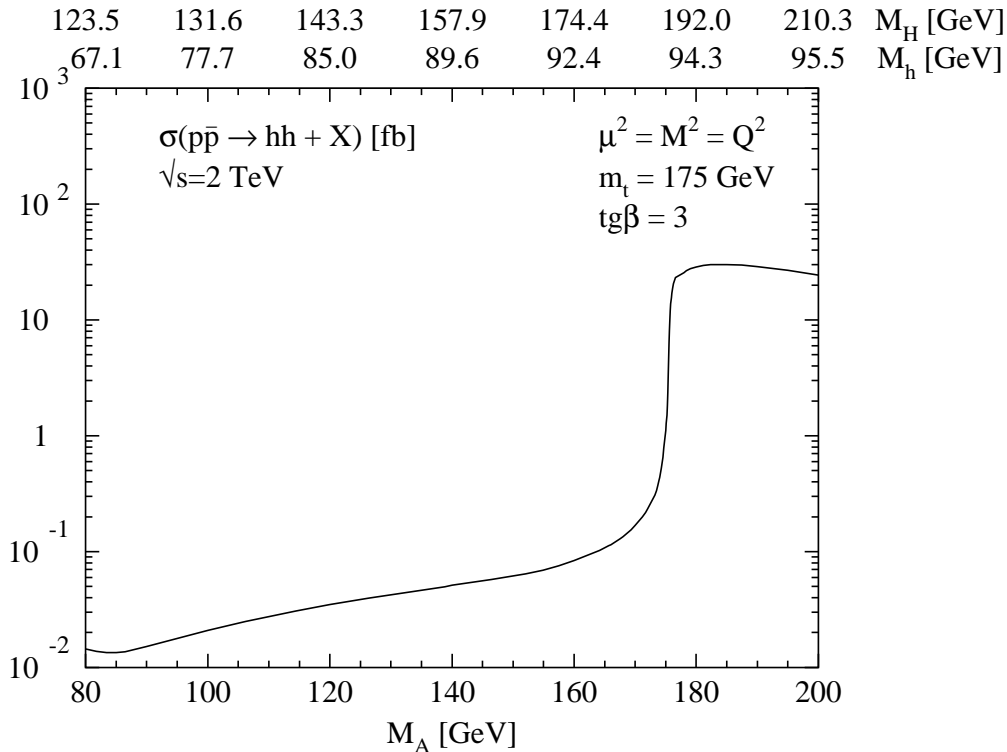
| 123.5 | 131.6 | 143.3 | 157.9 | 174.4 | 192.0 | 210.3 | M_H [GeV] |
| 67.1 | 77.7 | 85.0 | 89.6 | 92.4 | 94.3 | 95.5 | M_h [GeV] |

$\sigma(p\bar{p} \to hh + X)$ [fb]

$\sqrt{s}$=2 TeV

$\mu^2 = M^2 = Q^2$

m_t = 175 GeV

$tg\beta = 3$

M_A [GeV]

Figure 14: *Scalar Higgs-boson pair-production cross section $\sigma(p\bar{p} \to hh + X)$ at NLO as a function of the pseudoscalar Higgs mass M_A for $tg\beta = 3$ at the Tevatron $p\bar{p}$ collider with c.m. energy $\sqrt{s} = 2$ TeV.*

Moreover, we have shown that the NLO prediction of Higgs-boson pair production is sensitive to a deviation of the trilinear Higgs coupling from its SM value, rendering this process well suited for studying this coupling in *pp* collisions.

References

[1] P. W. Higgs, Phys. Lett. **12** (1964) 132 and Phys. Rev. **145** (1966) 1156;
F. Englert and R. Brout, Phys. Rev. Lett. **13** (1964) 321;
G. S. Guralnik, C. R. Hagen and T. W. Kibble, Phys. Rev. Lett. **13** (1964) 585.

[2] For reviews on the Higgs sector in the Standard Model and in its supersymmetric extensions, see J.F. Gunion, H.E. Haber, G.L. Kane and S. Dawson, *The Higgs*

Hunter's Guide (Addison–Wesley, Reading, Mass., 1990);
S. Dawson, preprint BNL-HET-SD-97-004, to be published in *Perspectives in Higgs Physics*, G. Kane, ed., hep-ph/9703387;
M. Spira and P.M. Zerwas, preprint CERN-TH/97-379, Lectures at *36th Internationale Universitätswochen für Kernphysik und Teilchenphysik*, Schladming 1997, hep-ph/9803257.

[3] Y. Okada, M. Yamaguchi and T. Yanagida, Prog. Theor. Phys. **85** (1991) 1;
H.E. Haber and R. Hempfling, Phys. Rev. Lett. **66** (1991) 1815;
J. Ellis, G. Ridolfi and F. Zwirner, Phys. Lett. **B257** (1991) 83.

[4] R. Hempfling and A. Hoang, Phys. Lett. **B331** (1994) 99;
S. Heinemeyer, W. Hollik and G. Weiglein, preprint KA-TP-2-1998, hep-ph/9803277.

[5] M. Carena, J.R. Espinosa, M. Quirós and C.E.M. Wagner, Phys. Lett. **B355** (1995) 209;
M. Carena, M. Quirós and C.E.M. Wagner, Nucl. Phys. **B461** (1996) 407.

[6] V. Barger, T. Han and R.J.N. Phillips, Phys. Rev. **D38** (1988) 2766.

[7] D.A. Dicus, K.J. Kallianpur and S.S.D. Willenbrock, Phys. Lett. **B200** (1988) 187;
A. Abbasabadi, W.W. Repko, D.A. Dicus and R. Vega, Phys. Rev. **D38** (1988) 2770;
Phys. Lett. **B213** (1988) 386.

[8] K.J. Kallianpur, Phys. Lett. **B215** (1988) 392.

[9] E.W.N. Glover and J.J. van der Bij, Nucl. Phys. **B309** (1988) 282.

[10] T. Plehn, M. Spira and P.M. Zerwas, Nucl. Phys. **B479** (1996) 46 and Erratum.

[11] A. Djouadi, talk at the Workshop *Theory of LHC Processes*, CERN, Geneva, 1998.

[12] M. Krämer, E. Laenen and M. Spira, Nucl. Phys. **B511** (1998) 523.

[13] A. Djouadi, M. Spira and P.M. Zerwas, Phys. Lett. **B264** (1991) 440;
S. Dawson, Nucl. Phys. **B359** (1991) 283.

[14] M. Spira, A. Djouadi, D. Graudenz and P.M. Zerwas, Nucl. Phys. **B453** (1995) 17.

[15] J. Ellis, M.K. Gaillard and D.V. Nanopoulos, Nucl. Phys. **B106** (1976) 292;
A.I. Vainshtein, M.B. Voloshin, V.I. Zakharov and M.A. Shifman, Sov. J. Nucl. Phys. **30** (1979) 711.

[16] B.A. Kniehl and M. Spira, Z. Phys. **C69** (1995) 77.

[17] S.L. Adler, Phys. Rev. **177** (1969) 2426;
J.S. Bell and R. Jackiw, Nuovo Cimento **60A** (1969) 47.

[18] A. Djouadi, M. Spira and P.M. Zerwas, Phys. Lett. **B311** (1993) 255;
M. Spira, A. Djouadi, D. Graudenz and P.M. Zerwas, Phys. Lett. **B318** (1993) 347;
R.P. Kauffman and W. Schaffer, Phys. Rev. **D49** (1994) 551.

[19] S.L. Adler and W.A. Bardeen, Phys. Rev. **182** (1969) 1517;
R. Jackiw, *Lectures on Current Algebra and its Applications* (Princeton University Press, 1972).

[20] G. Altarelli and G. Parisi, Nucl. Phys. **B126** (1977) 298.

[21] J. Küblbeck, M. Böhm and A. Denner, Comput. Phys. Commun. **60** (1990) 165;
H. Eck and J. Küblbeck, *Guide to FeynArts 1.0*, University of Würzburg, 1992.

[22] V.A. Smirnov, Phys. Lett. **B394** (1997) 205.

[23] S.G. Gorishny, Nucl. Phys. **B319** (1989) 633;
V.A. Smirnov, Commun. Math. Phys. **134** (1990) 109; *Renormalization and asymptotic expansions* (Birkhäuser Verlag, Basel, 1991);
F.V. Tkachov, Int. J. Mod. Phys. **A8** (1993) 2047;
G.B. Pivovarov and F.V. Tkachov, Int. J. Mod. Phys. **A8** (1993) 2241.

[24] S. Wolfram, *Mathematica — A System for Doing Mathematics by Computer* (Addison-Wesley, Redwood City, CA, 1988).

[25] G. 't Hooft and M. Veltman, Nucl. Phys. **B44** (1972) 189;
P. Breitenlohner and D. Maison, Commun. Math. Phys. **52** (1977) 11.

[26] W. Furmanski and R. Petronzio, Z. Phys. **C11** (1982) 293 and references therein.

[27] H.L. Lai, J. Huston, S. Kuhlmann, F. Olness, J. Owens, D. Soper, W.K. Tung and H. Weerts, Phys. Rev. **D55** (1997) 1280.

[28] G.J. Gounaris, D. Schildknecht and F.M. Renard, Phys. Lett. **B83** (1979) 191; (E) **B89** (1980) 437;
J.F. Gunion, L. Roszkowski, A. Turski, H.E. Haber, G. Gamberini, B. Kayser, S.F. Novaes, F. Olness and J. Wudka, Phys. Rev. **D38** (1988) 3444;
V. Barger and T. Han, Mod. Phys. Lett. **A5** (1990) 667;
F. Boudjema and E. Chopin, Z. Phys. **C73** (1996) 85.

[29] E. Richter-Was, D. Froidevaux, F. Gianotti, L. Poggioli, D. Cavalli and S. Resconi, preprint CERN-TH/96-111.

[30] For recent reviews, see e.g. A. Djouadi, Int. J. Mod. Phys. **A10** (1995) 1;
M. Spira, Fortschr. Phys. **46** (1998) 203.

[31] A. Djouadi, H.E. Haber and P.M. Zerwas, Phys. Lett. **B375** (1996) 203.